THE ASTROPHYSICAL JOURNAL, 295:422–436, 1985 August 15

MASSACHUSETTS–STONY BROOK GALACTIC PLANE CO SURVEY: THE GALACTIC DISK ROTATION CURVE

DAN P. CLEMENS[1]
Five College Radio Astronomy Observatory; and Department of Physics and Astronomy, University of Massachusetts, Amherst; and Steward Observatory, University of Arizona
Received 1984 October 3; accepted 1985 February 25

ABSTRACT

Data from the Massachusetts–Stony Brook Galactic plane CO survey have been analyzed to determine the dependence of CO radial velocity on Galactic longitude along the loci of tangents in the inner Galaxy. These measurements are combined with published data for H I in the nuclear region, outer Galaxy CO–H II regions, and the globular cluster system to yield a rotation curve valid over the northern Galactic disk. Streaming motions characterized by lengths larger than 0.22 R_0 and velocities of 5 km s^{-1} have been successfully separated from the smaller scale cloud-cloud motions, which possess linear scale lengths up to 0.015 R_0 and one-dimensional velocity dispersions of 3.0 km s^{-1}. The LSR exhibits an azimuthal peculiar velocity of 7 km s^{-1}.

Subject headings: galaxies: internal motions — galaxies: Milky Way — interstellar: molecules

I. INTRODUCTION

An accurate rotation curve for the Milky Way Galaxy is crucial to constraining models of the Galactic mass components and to assigning kinematic distances to Galactic objects. The derivation of this curve lies principally in the domain of spectral line radio astronomy, as matter throughout the Galaxy must be sampled. The first rotation curve derived for the whole Milky Way was that of Kwee, Muller, and Westerhout (1954), who analyzed the dependence of the maximum observed radial velocity of H I emission on Galactic longitude. Since then, numerous authors have obtained higher resolution (spectral and spatial) atomic hydrogen data to refine this tangent point method.

The advent of CO as a tracer of the denser, molecular hydrogen component of the interstellar medium enabled Burton and Gordon (1978, hereafter BG) to demonstrate that the H I gas and CO clouds exhibit almost identical Galactic kinematics, in both their large-scale motions and in their deviations from circular rotation. Their rotation curve was derived from the H I data of Westerhout (1976), however, and not their own observations of CO.

The rotation of the outer Galaxy has been studied by direct measurement of the distances to the exciting stars in optical H II regions by Jackson, FitzGerald, and Moffat (1979). Their optically determined velocities have been improved by CO observations of the molecular clouds associated with the H II regions by Blitz (1979) and Blitz, Fich, and Stark (1980). The rotation curves derived from these data show, contrary to the Schmidt (1965) model, that the rotation speed beyond the solar circle does not decrease in a Keplerian fashion, indicative of a galaxy dominated by nuclear, disk, and spheroidal components, but rather is flat or rising, probably requiring a massive halo. Similar rotation curves suggesting massive halos seem to be typical of Sb and Sc galaxies (Rubin, Ford, and Thonnard 1978; Rubin *et al.* 1982).

The recent completion of the Massachusetts–Stony Brook CO survey of the northern inner Galactic plane (Sanders *et al.* 1985) has greatly increased the size of the CO data base available for a rotation curve analysis. In this paper a rotation curve for the northern Milky Way is presented which is based on these CO data, H I data of the nuclear region ($R < 0.3\ R_0$) from Westerhout (1976) as analyzed by BG, outer Galaxy CO–H II region data from Blitz, Fich, and Stark (1982), and the mass of the Galaxy to 60 kpc as inferred from the globular cluster system by Hartwick and Sargent (1978). The nature of the deviations away from the smooth curve are analyzed and the relative importance of streaming motions and cloud-cloud motions are assessed.

II. DATA

a) CO *Tangent Point Detection*

The full details of the CO survey data collection and equipment are described elsewhere (Sanders *et al.* 1985). The information relevant to this study are the l and b coverages, spectral and spatial resolution, and baseline noise level of the survey data. The beamwidth of the FCRAO[2] 14 m telescope was 45″ at the 115 GHz CO line frequency. Galactic longitudes between 18° and 55° were sampled on a 3′ × 3′ grid from $b = -1.^\circ05$ to $1.^\circ00$. A 6′ × 6′ grid was used for $l = 8°$ to $17.^\circ9$ and $l = 55.^\circ1$ to $89.^\circ9$, both from $b = -1°$ to $+1°$. The data were obtained using a 512 channel by 250 kHz filter bank and smoothed to 1 km s^{-1} resolution. The resulting spectra were truncated to 301 km s^{-1} width, and typically cover velocities (LSR) of -100 to 200 km s^{-1}. The baseline noise level is 0.41 K (T_R*) rms.

Each spectrum of the full CO survey data set (40,551 spectra) was checked for the presence of a CO emission line within ±15 km s^{-1} of the BG rotation curve velocity. A line was presumed detected if each of three consecutive 1 km s^{-1} channels registered CO emission stronger than 1.2 K (3 σ). This three-channel test was stepped across the 30 km s^{-1} window to find

[1] Bart J. Bok Fellow, 1984–1985.

[2] The Five College Radio Astronomy Observatory is operated with support from the National Science Foundation under grant AST 82-12252 and with permission of the Metropolitan District Commission, Commonwealth of Massachusetts.

the highest velocity line in each spectrum. The velocity assigned is the one associated with the highest velocity of the three channels. This channel straddles the high-velocity wing of the CO line, while the other two channels verify that a line is actually present.

To find the velocity of the cloud, instead of the velocity associated with the high-velocity wing, the measured velocity is corrected by the half-width to 1.2 K for an average tangent point cloud. This correction is 3.0 ± 1.5 km s^{-1}, based on the following arguments. Sanders, Scoville, and Solomon (1985) find that clouds with diameters between 20 and 80 pc have a CO line width spectrum and a cloud size spectrum which can be approximated as power laws of the cloud diameter ($\Delta V_{\rm FWHM} \approx D^{0.62}$, $N(D) \approx D^{-2.32}$). If these relations hold down to the smallest mean sizes sampled by the present survey (~ 5 pc), then the average CO tangent cloud possesses a line width (FWHM) of about 5 ± 2 km s^{-1}. Sanders (1981) found the average peak CO temperature for Galactic clouds of diameter 10–20 pc to be 5 ± 1.5 K (T_R*). When the average CO line observed is modeled as Gaussian, the desired correction is 3.5 ± 1.5 km s^{-1} (or less, since the temperature of the high-velocity channel of the three-channel test must be *greater* than 1.2 K). However, CO lines are optically thick in molecular clouds, and the direction of the departure away from Gaussian shape reduces the correction. The value cannot be *less* than the HWHM, ~ 2.5 km s^{-1}, if the velocity discriminant is sensitive to positions on the line profile below the half-maximum emission value. For these reasons, a correction of 3.0 ± 1.5 km s^{-1} has been adopted as the nominal value. Previous works have used similar corrections: using the equivalent-rectangular tangent point measurement scheme (Shane and Bieger-Smith 1966), BG corrected their measures down by 2.5 km s^{-1} to obtain tangent velocities, and Liszt, Xiang, and Burton (1981) similarly reduced their ^{13}CO velocities by 1.3 km s^{-1}.

b) *Different Latitude Samples*

The highest velocity CO line along any direction need not arise from tangent point gas: because CO emission comes from discrete clouds, not all lines of sight will pierce clouds at the tangent point. Clouds nearer or further than the tangent point may actually contribute the highest velocity lines to an observed spectrum within the ± 15 km s^{-1} velocity window. The nearer clouds may possess somewhat larger angular z-heights than the tangent clouds, and both nearer and farther clouds will have velocities lower than those associated with the tangent point. Although clouds in pure circular rotation with velocities 15 km s^{-1} lower than the tangent velocity have scale heights similar to the tangent gas over much of the tangent circle, closer noncircular clouds may fall within the velocity window. By forming subsets of the data, characterized by different z-extents, some of these contaminating clouds may be identified and removed from the rotation analysis.

The location of the CO midplane with respect to $b = 0°$, Z_0, and the thickness of the CO gas layer in the z-direction σ_z were determined along the loci of tangents by Sanders, Solomon, and Scoville (1984). Useful approximations to their findings are

$$Z_0(\text{pc}) = 0\,, \qquad l < 37°\,, \tag{1}$$
$$= R_0(0.0222 \sin l - 0.0193)\,, \quad l > 37°\,,$$

$$\sigma_z(\text{pc}) = R_0(0.0043 \sin l + 0.0026)\,. \tag{2}$$

Four samples were obtained from the CO survey data, characterized by latitude extents of $\pm 0.5\sigma_z$, $\pm 1\sigma_z$, and $\pm 2\sigma_z$ away from the CO midplane latitude, and one latitude-unrestricted sample. The characteristics of these samples are listed in Table 1. In column (4) the fraction of the allowed positions detected is seen to rise as the latitude range is reduced, as expected for a cloud distribution which peaks at the CO midplane. The detection fraction saturates at about $\frac{2}{3}$, indicating that the CO emission is patchy and arises from well-separated clouds. Since the likelihood of detecting a line in the velocity window along any direction is less than $\frac{2}{3}$, the chance of having *two* tangent clouds contributing lines to one spectrum must be less than $(\frac{2}{3})^2$. To actually miss the lower velocity cloud altogether requires that it have a smaller extent in all (l, b)-directions than the higher velocity cloud. Removing the latitude restriction reduces this "shielding" problem even more. Hence the survey data set and the tangent velocity selection method described enable detecting almost all CO clouds larger than 5–6 pc along the loci of tangents.

When the data from any of the four samples are plotted, two aspects are apparent. The first is the small amount of velocity scatter over small regions of longitude, and the second is the presence of large-scale velocity deviations or features which extend over several degrees. The small-scale scatter is a reflection of the small cloud-cloud motions present, while the larger scale motions are similar to those hypothesized as streaming associated with spiral density waves (Yuan 1969).

c) *Recovering the Tangent Velocities*

In addition to forming restricted latitude samples, the contamination of the tangent point data by nontangent clouds may be reduced by analyzing the distribution of measured velocities. In a volume of space closely surrounding a tangent

TABLE 1

CHARACTERISTICS OF THE LATITUDE SAMPLES

Sample Type (1)	Number of Lines Detected (2)	Fraction of Total[a] (3)	Fraction of Allowed[b] (4)	Fraction of Bins with Two Gaussians (5)	Dispersion (km s^{-1})[c] (6)
... .	17586	0.434	0.434	0.23	3.2 ± 0.8
$\pm 2\sigma_z$	16429	0.405	0.550	0.20	3.1 ± 0.7
$\pm 1\sigma_z$	11832	0.292	0.644	0.12	2.7 ± 0.6
$\pm 0.5\sigma_z$	6471	0.159	0.644	0.04	2.3 ± 0.5

[a] Fraction of the total survey positions, 40,551, detected by the three-channel test within ± 15 km s^{-1} of the BG rotation curve value.

[b] Fraction of survey positions detected within the specified z-extent of the CO midplane.

[c] Mean dispersion of tangent point Gaussian component of $N(v)$. Errors are probable errors, 0.67 σ.

point, the true tangent clouds will have some average galactic rotational velocity and a random, cloud-cloud velocity. A similar volume *not* at the tangent point will possess a sample of clouds with a different (lower) mean radial velocity. The tangent point velocity may be found by binning the observed velocities from a small longitude range and examining the resulting histogram of velocities.

The data from each of the four latitude samples were placed in bins of equal $\Delta \sin l = 0.005$, corresponding to $\Delta R = 50$ pc for $R_0 = 10$ kpc. The velocity histogram $N(v)$, with channel resolution of 2 km s^{-1}, was formed for each of these longitude bins and fitted using one or two Gaussians. Figure 1 shows $N(v)$ for the four samples in the longitude bin at $l = 31.^{\circ}50$ and the Gaussians fit to the distributions. Longitude bins containing fewer than four total lines were excluded from fitting and further analysis. Second Gaussian fitting was only performed on those longitude bins which had residuals after single Gaussian fitting which exceeded 3 σ (Poisson errors) and extended over two or more 2 km s^{-1} velocity channels.

The fraction of longitude bins showing two Gaussian components is listed in column (5) of Table 1 for each latitude sample. As the samples are restricted in latitude, the second Gaussian dissappears from the $N(v)$ distributions. Since this component is usually at a lower velocity than the first Gaussian ($\langle V_1 - V_2 \rangle = 11 \pm 2$ km s^{-1}) and exhibits a larger angular latitude extent than the first, this second component is probably due to clouds closer to the Sun than the tangent point. Some clouds farther away than the tangent point will still contribute to the samples even with reduction of the latitude extents. However, as they will contribute preferentially to the low-velocity component, the high-velocity Gaussian is identified as arising from the true tangent point. A small number of longitude bins showed a high-velocity component which was weaker (possessed fewer lines) than the low-velocity component and was present only in the large latitude samples. For these cases, the lower velocity component which persisted to low latitude ranges was considered to be the tangent point component.

This Gaussian tangent point component of the $N(v)$ distributions in each spatial bin contains information about the velocities of the CO clouds in the volume of the Galaxy corresponding to that bin. If within each such volume every cloud at the tangent point contributes just one velocity to $N(v)$, the mean velocity of this distribution must be the mean of the CO cloud velocities and the dispersion of the distribution related to the value of the random motions of the clouds. Hence the center velocity of the Gaussian fit to the high-velocity component in each spatial bin is the tangent point velocity for that bin. Similarly, the dispersion of the Gaussian is associated with the cloud-cloud dispersion σ_{cc}, as shown below. Column (6) in Table 1 lists the mean fitted σ_{cc} and probable errors for each of the four samples, assuming σ_{cc} has no variation with Galactic radius (but see discussion in next section).

When the latitude extent decreases below $\pm 2\sigma_z$, the cloud-cloud dispersion also decreases. This seems to indicate that these motions are correlated up to such a length scale. Variation of the longitudinal bin width affects σ_{cc} in the same fashion. Holding the allowed latitude extent constant at $\pm 1\sigma_z$, the tangent velocities were put into bins of $\Delta \sin l = 0.01$ and 0.0025 width. The dispersions found were 3.2 ± 0.6 km s^{-1} for the larger bins and 2.3 ± 0.6 km s^{-1} for the smaller. Galactic shear alone cannot account for the magnitude of the dispersions observed, nor the way in which the dispersions marginally vary with bin size. Cloud-cloud motions, possessing one-dimensional velocity dispersions of 3.0 ± 0.7 km s^{-1}, and linear correlation lengths up to about 0.015 R_0, are present in the sample of clouds along the loci of tangents.

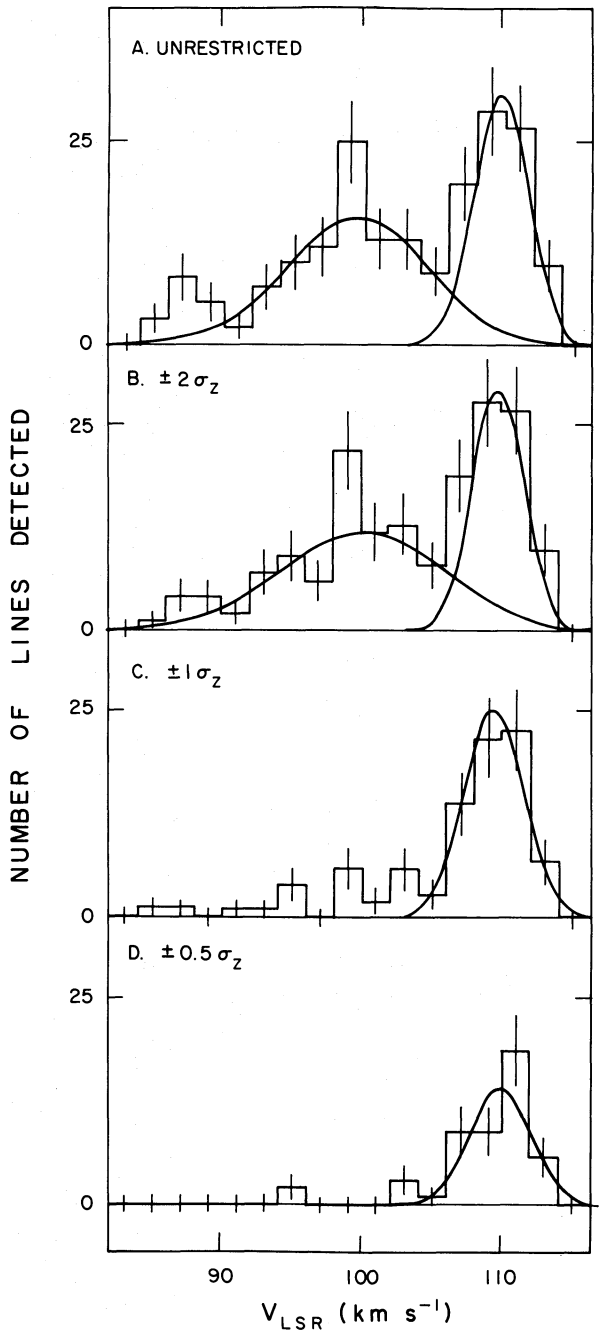

FIG. 1.—Plots of $N(v)$ and Gaussian fits for the longitude bin at $31.^{\circ}50$. (*a*) Unrestricted sample; (*b*) $\pm 2\sigma_z$ sample; (*c*) $\pm 1\sigma_z$ sample; (*d*) $\pm 0.5\sigma_z$ sample. Note the disappearance of the second Gaussian component as the latitude range is reduced.

The final data used for the rotation curve analysis are listed in Table 2. There, the bin center longitudes for the $\Delta \sin l = 0.005$, $\pm 1\sigma_z$ sample are listed, along with the number of lines detected in each bin and the Gaussian fit parameters and errors for the tangent velocity component seen in the $N(v)$

distributions for each bin. The subtraction of 3 km s^{-1} to bring each bin's velocity at 1.2 K to the tangent velocity has *not* been included in the table.

d) LSR Motion

The line center velocities and errors from Table 2 are plotted versus Galactic radius ($R/R_0 = \sin l$) in Figure 2. This figure may be compared directly to the corresponding H I figure shown by Gunn, Knapp, and Tremaine (1979, hereafter GKT). Their linear fit to the H I data in the region from 0.5 to 1.0 R_0 was used to estimate the H I dispersion and the value of AR_0. However, in Figure 2, the two regions which are reasonably clear of large-scale motions, namely 0.62–0.73 and 0.81–0.97 R_0, have slopes which differ at the 10 σ level. Consequently, to estimate the mean tangent velocity at R_0, which is a measure of the noncircular motion of the LSR, the latter region, 0.81–0.97

TABLE 2

CO TANGENT POINT DATA USED IN THE ROTATION CURVE

ℓ[a] (°)	N[b]	$V_{tangent}$[c] (km s^{-1})	σ_{cc}[c] (km s^{-1})	ℓ (°)	N	$V_{tangent}$ (km s^{-1})	σ_{cc} (km s^{-1})	ℓ (°)	N	$V_{tangent}$ (km s^{-1})	σ_{cc} (km s^{-1})
13.44	7	156.32 (4.88)	6.96 (4.75)	32.51	79	98.92 (0.21)	2.30 (0.16)	51.95	158	60.93 (0.30)	4.20 (0.22)
14.92	5	140.99 (0.67)	1.74 (0.61)	32.85	89	99.45 (0.40)	4.43 (0.28)	52.42	185	62.81 (0.23)	2.34 (0.18)
17.01	5	130.56 (1.49)	2.94 (1.49)	33.20	79	97.77 (0.77)	7.48 (0.64)	52.89	179	62.26 (0.15)	2.42 (0.10)
17.61	5	134.37 (1.59)	8.70 (1.70)	33.54	82	107.74 (0.22)	1.66 (0.15)	53.37	109	63.61 (2.07)	1.78 (1.54)
17.91	6	129.53 (0.45)	2.37 (0.48)	33.88	75	102.88 (1.80)	3.44 (1.50)	53.85	100	56.28 (0.37)	4.13 (0.28)
18.21	19	127.69 (0.25)	1.37 (0.22)	34.23	70	107.55 (1.74)	2.61 (1.56)	54.34	111	39.63 (0.38)	2.83 (0.32)
18.51	29	127.57 (0.29)	1.89 (0.25)	34.58	78	98.09 (0.25)	1.94 (0.23)	54.84	68	41.16 (0.21)	2.35 (0.15)
18.81	34	123.61 (0.56)	2.84 (0.52)	34.92	79	85.82 (0.54)	5.39 (0.45)	55.34	36	40.62 (0.58)	3.84 (0.49)
19.12	34	124.85 (0.22)	1.76 (0.21)	35.27	79	83.60 (0.33)	3.61 (0.27)	55.84	40	41.02 (0.81)	5.03 (0.69)
19.42	30	123.56 (0.34)	2.15 (0.31)	35.63	85	84.52 (0.66)	2.39 (0.61)	56.36	54	39.79 (0.42)	3.85 (0.36)
19.72	34	123.02 (0.27)	2.10 (0.21)	35.98	77	85.44 (0.28)	2.46 (0.19)	56.88	29	37.82 (0.77)	4.64 (0.70)
20.03	25	120.76 (0.48)	2.96 (0.41)	36.33	90	84.33 (0.28)	3.57 (0.27)	57.41	34	38.61 (0.39)	2.94 (0.36)
20.33	37	120.09 (0.67)	3.81 (0.52)	36.69	94	87.56 (0.28)	3.12 (0.19)	57.94	49	36.12 (0.77)	5.14 (0.61)
20.64	42	122.51 (0.47)	3.53 (0.46)	37.05	82	85.14 (0.22)	2.62 (0.19)	58.48	36	41.39 (0.52)	3.56 (0.48)
20.95	24	118.78 (1.03)	4.62 (0.84)	37.41	96	84.62 (0.40)	4.32 (0.30)	59.04	53	27.61 (0.23)	1.90 (0.20)
21.25	61	120.50 (0.59)	5.49 (0.48)	37.77	108	89.51 (0.29)	3.05 (0.22)	59.60	41	30.45 (0.50)	3.92 (0.40)
21.56	47	120.41 (0.52)	4.24 (0.40)	38.13	92	85.62 (0.87)	6.73 (0.64)	60.17	28	29.04 (0.38)	2.43 (0.31)
21.87	34	111.82 (0.79)	5.34 (0.68)	38.50	99	86.12 (0.37)	4.02 (0.27)	60.75	19	32.50 (0.64)	1.64 (0.65)
22.18	49	115.76 (0.54)	4.48 (0.45)	38.87	105	85.56 (0.18)	2.49 (0.14)	61.34	24	23.05 (0.30)	1.72 (0.25)
22.49	66	117.37 (0.49)	4.40 (0.37)	39.23	120	83.17 (0.18)	2.76 (0.13)	61.95	22	30.80 (0.57)	2.69 (0.49)
22.80	74	114.13 (0.53)	5.27 (0.41)	39.61	102	84.80 (0.19)	2.51 (0.17)	62.56	33	26.71 (1.20)	6.25 (1.18)
23.11	59	112.65 (0.59)	5.27 (0.48)	39.98	121	81.74 (0.28)	4.13 (0.22)	63.19	34	26.87 (0.58)	4.14 (0.47)
23.42	66	108.68 (0.40)	4.19 (0.32)	40.35	91	78.86 (0.25)	3.28 (0.20)	63.83	18	22.97 (0.86)	4.07 (0.75)
23.73	64	111.34 (0.52)	5.37 (0.47)	40.73	104	75.00 (0.48)	5.25 (0.33)	64.49	27	23.16 (0.27)	1.59 (0.22)
24.05	74	115.31 (0.33)	3.51 (0.26)	41.11	101	78.00 (0.27)	3.38 (0.22)	65.16	20	17.75 (0.75)	3.39 (0.62)
24.36	66	119.07 (0.45)	4.26 (0.36)	41.49	114	74.79 (0.21)	3.10 (0.16)	65.85	31	19.96 (0.43)	2.59 (0.33)
24.68	65	113.86 (0.36)	3.74 (0.32)	41.87	127	74.20 (0.19)	2.98 (0.13)	66.56	35	18.02 (0.49)	3.45 (0.40)
24.99	59	109.42 (0.27)	2.74 (0.22)	42.26	128	71.39 (0.23)	3.27 (0.21)	67.29	13	12.43 (0.57)	2.37 (0.55)
25.31	72	109.31 (0.29)	3.40 (0.23)	42.65	115	70.32 (0.20)	2.91 (0.15)	68.05	5	16.23 (2.84)	4.99 (2.91)
25.63	66	111.34 (0.27)	2.33 (0.19)	43.04	118	65.44 (0.18)	2.61 (0.13)	68.83	26	14.66 (0.69)	3.62 (0.65)
25.94	76	110.30 (0.46)	4.94 (0.38)	43.43	111	66.38 (0.26)	3.69 (0.19)	69.64	23	17.85 (1.58)	5.60 (1.39)
26.26	61	110.78 (0.44)	4.09 (0.33)	43.83	109	66.04 (0.27)	3.67 (0.19)	70.48	56	12.26 (0.18)	1.97 (0.15)
26.58	61	107.43 (0.61)	5.62 (0.50)	44.23	132	67.07 (0.19)	2.78 (0.14)	71.35	56	11.71 (0.15)	1.59 (0.13)
26.90	71	105.80 (0.55)	5.76 (0.47)	44.63	145	67.38 (0.20)	3.38 (0.16)	72.27	37	6.03 (0.17)	1.24 (0.13)
27.23	62	104.01 (0.33)	3.54 (0.31)	45.03	121	68.88 (0.16)	1.94 (0.12)	73.24	46	5.15 (0.16)	1.56 (0.13)
27.55	68	105.27 (0.42)	4.45 (0.35)	45.44	134	64.84 (0.20)	3.27 (0.16)	74.26	56	6.21 (0.29)	2.80 (0.22)
27.87	65	103.89 (0.18)	2.04 (0.13)	45.85	151	64.54 (0.16)	2.69 (0.13)	75.35	79	2.60 (0.35)	3.95 (0.27)
28.20	87	106.26 (0.33)	4.14 (0.26)	46.26	136	62.54 (0.23)	3.79 (0.19)	76.53	113	1.00 (0.25)	3.53 (0.21)
28.52	76	106.34 (0.31)	3.37 (0.22)	46.68	115	61.05 (0.23)	3.50 (0.19)	77.82	229	2.61 (0.32)	2.95 (0.22)
28.85	89	105.64 (0.42)	4.54 (0.29)	47.10	100	60.86 (0.39)	4.76 (0.32)	79.27	265	11.25 (0.13)	2.25 (0.10)
29.18	76	100.25 (0.15)	1.78 (0.12)	47.52	60	55.25 (1.71)	7.80 (1.47)	80.93	294	8.36 (0.46)	1.99 (0.29)
29.51	90	102.46 (0.34)	3.87 (0.26)	47.94	113	57.80 (0.23)	2.35 (0.20)	82.98	269	8.68 (0.21)	4.18 (0.14)
29.83	75	107.55 (0.21)	2.31 (0.16)	48.37	114	58.29 (0.22)	3.15 (0.16)	85.95	330	4.08 (0.10)	2.07 (0.09)
30.17	90	109.48 (0.25)	3.06 (0.21)	48.81	143	61.14 (0.42)	6.05 (0.32)				
30.50	91	110.05 (0.36)	3.64 (0.27)	49.24	163	66.63 (0.21)	3.65 (0.16)				
30.83	78	109.37 (0.32)	3.01 (0.24)	49.69	163	67.47 (0.15)	2.56 (0.12)				
31.16	90	110.11 (0.19)	2.40 (0.15)	50.13	131	47.56 (0.24)	1.92 (0.20)				
31.50	91	109.93 (0.18)	2.16 (0.14)	50.58	167	48.07 (0.30)	2.82 (0.24)				
31.84	81	106.70 (0.38)	4.23 (0.29)	51.03	171	60.59 (0.25)	4.25 (0.22)				
32.17	64	99.50 (0.13)	1.28 (0.10)	51.49	173	59.80 (0.21)	3.60 (0.16)				

[a] Longitude of bin center.
[b] Number of lines in bin.
[c] Errors are probable errors, 0.67 σ.

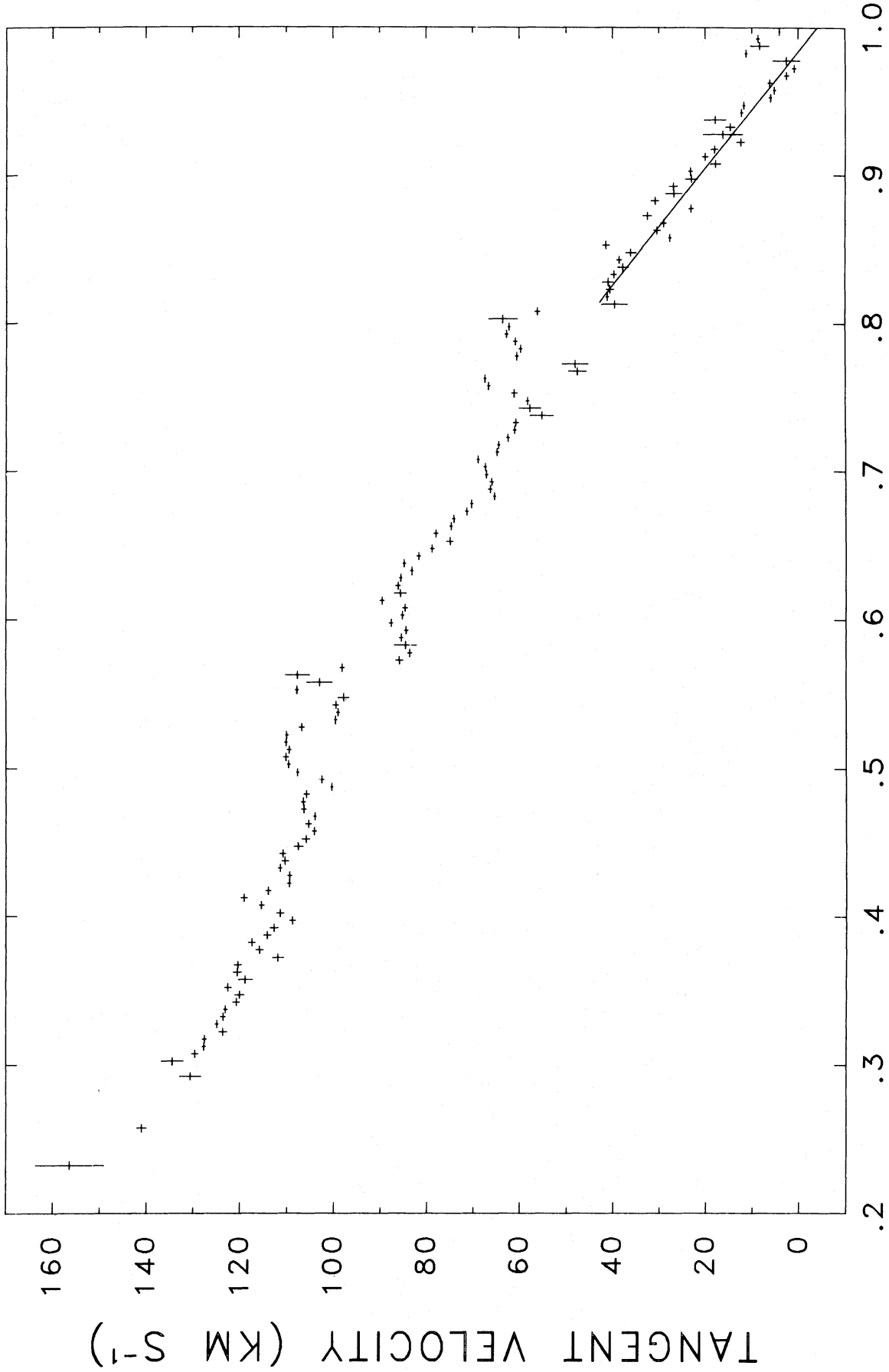

FIG. 2.—Plot of tangent point velocities, from Table 2, uncorrected for line width effects, vs. Galactic radius. Vertical error bars are from the Gaussian fits, and horizontal error bars indicate bin width. The straight line is the fit to the region from 0.81 to 0.97 R_0, which has an intercept of -4.0 ± 0.1 km s^{-1} and a slope ($-2.4R_0$) of -252 ± 1.1 km s^{-1}.

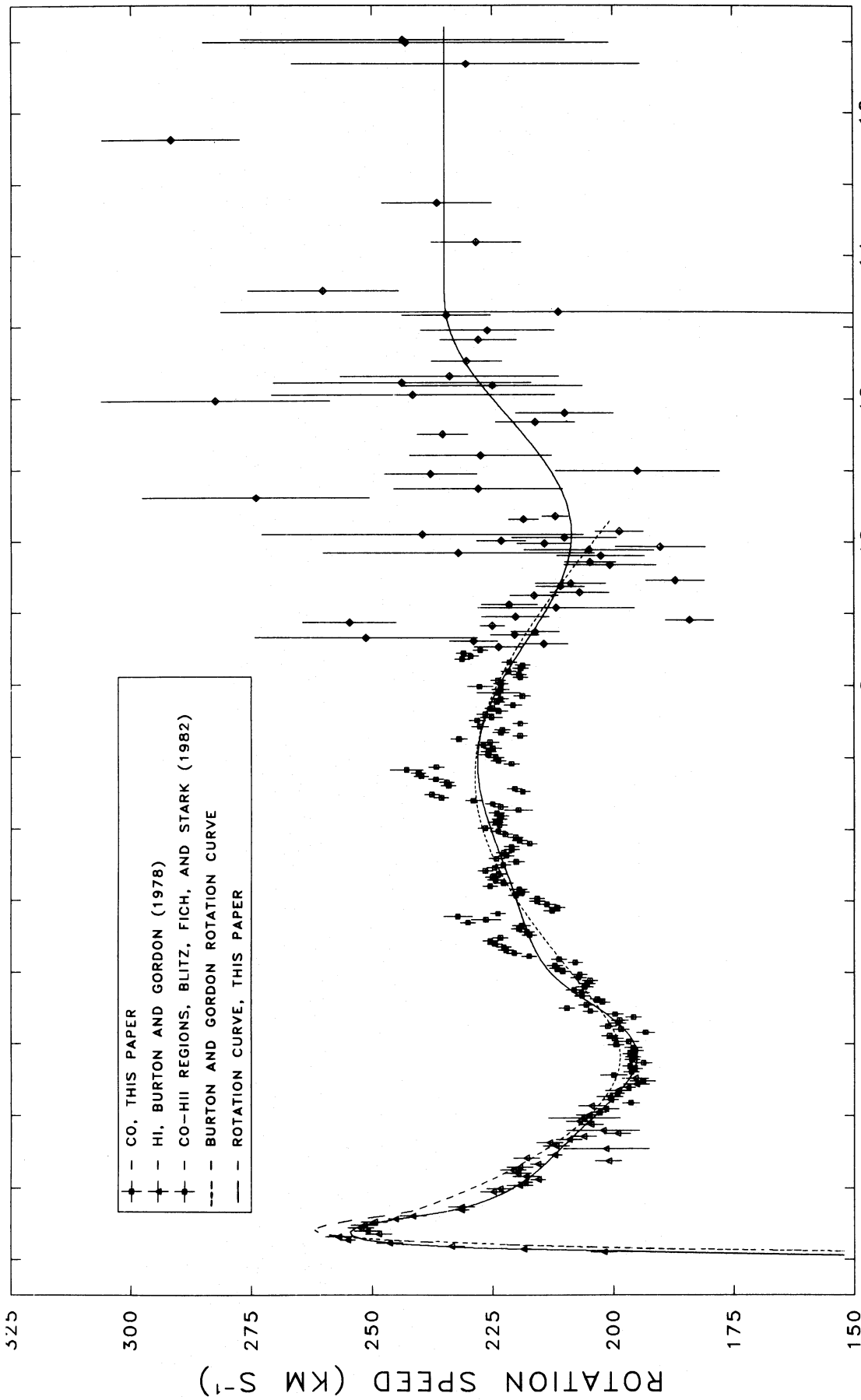

FIG. 3.—Plots of the rotation speed versus galactocentric radius. The solid lines correspond to the polynomials, and the dashed lines are the BG rotation curve. (*upper panel*)(R_0, θ_0) = (10 kpc, 220 km s^{-1}); (*lower panel*) (8.5 kpc, 220 km s^{-1}).

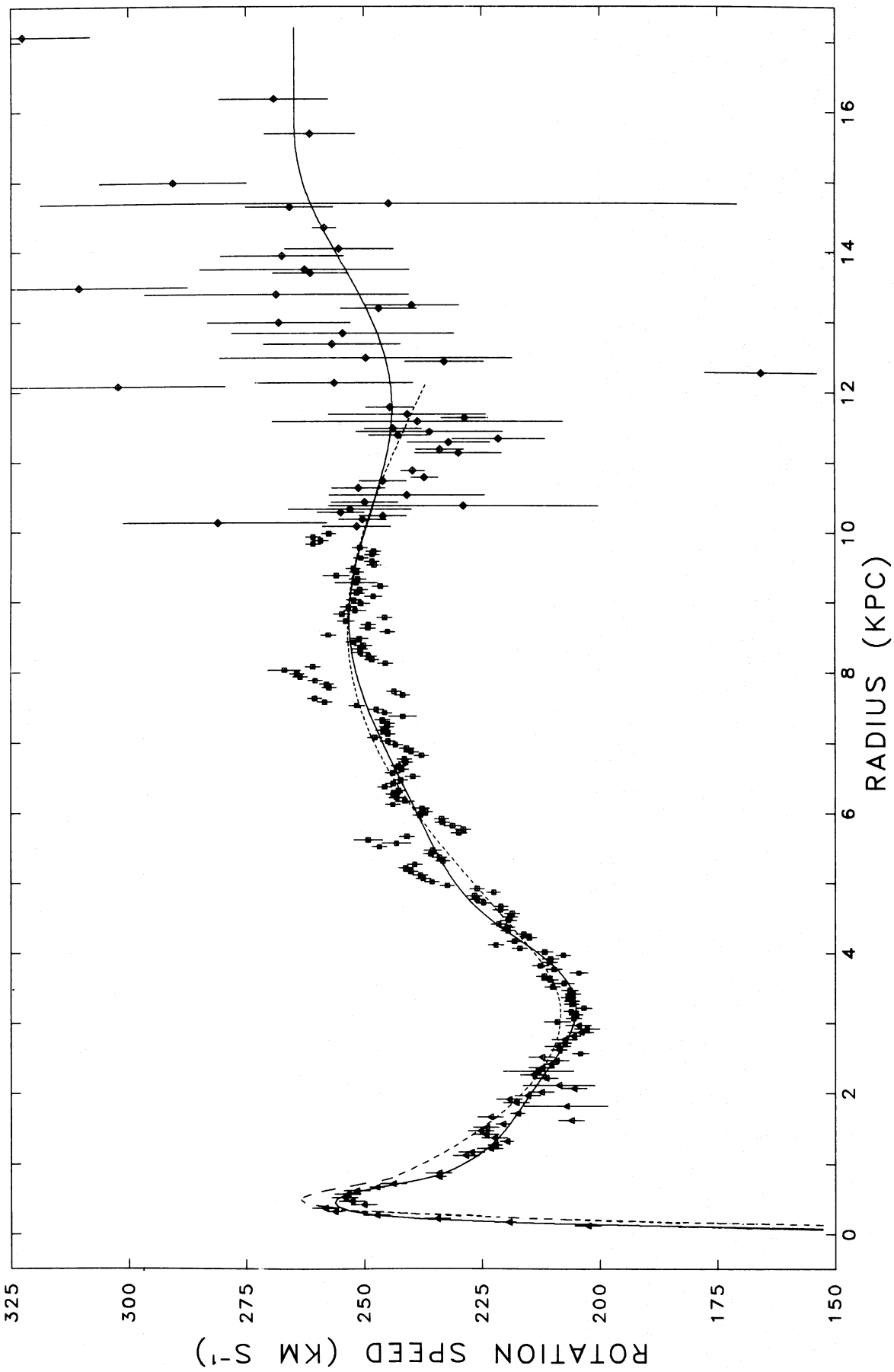

R_0, alone was fitted. The line in Figure 2 shows the fit and the extrapolation to R_0. Without the 3 km s^{-1} line width correction applied, the tangent velocity obtained at R_0 is -4.0 ± 0.1 km s^{-1}. Including the correction and its associated uncertainty brings the value to -7 ± 1.5 km s^{-1}. The slope of the line, -252 ± 1.1 km s^{-1}, leads to a value of AR_0 of 126 ± 0.6 km s^{-1}, somewhere between the GKT value of 110 km s^{-1} and the IAU adopted value of 150 km s^{-1}.

That the LSR is not in perfect circular motion about the center of the Galaxy has been inferred previously from the differences between the northern and southern H I rotation curves (Kerr 1962). Recently, Shuter (1982) used available H I and CO data to infer peculiar motions of 4–7 km s^{-1} in the radial (anticenter) direction and 6.8–8.5 km s^{-1} in the azimuthal direction. The agreement of his azimuthal motion with that determined above is good. However, the radial motion cannot be found using the northern CO data alone. Therefore, the combined northern and southern Galactic plane CO data of Robinson *et al.* (1984) were analyzed to determine the radial component of the LSR motion. Although these data do show differences between the tangent velocities at many longitudes for the two hemispheres, *the differences are not well fitted by the expected* cos l *form.* Hence the radial LSR motion is not well characterized and the remaining analysis in this paper assumes only a peculiar LSR motion of 7 ± 1.5 km s^{-1} in the azimuthal direction $l = 90°$.

III. COMBINED ROTATION CURVE

The Gaussian center velocities from Table 2 were corrected for line width and peculiar LSR motion effects and converted to linear rotation speeds θ and galactocentric radii R via

$$\theta(R) = \theta_0 \sin l + V_{\text{tangent}} , \quad (3)$$

$$R = R_0 \sin l . \quad (4)$$

For longitudes less than 15°–18°, CO becomes a poor tracer of the tangent emission because the abundance of molecular hydrogen has decreased by about an order of magnitude with respect to that found in the molecular ring (Sanders, Solomon, and Scoville 1984). Although atomic hydrogen is still less abundant than its molecular form in this region, its abundance *change* is smaller and is thereby better able to identify tangent velocities. The H I data of Westerhout (1976), as analyzed by BG, were used for those longitudes below 19° having no viable CO Gaussian components at the tangent point. These H I velocities were reduced by 4 km s^{-1} in addition to the peculiar LSR motion correction to enable agreement between the tangent point detection scheme used by BG and that used here (see § IV).

The $R > R_0$ "kinematically distinct" CO–H II region data of Blitz, Fich, and Stark (1982) were corrected for the peculiar LSR motion and converted to θ and R. The Galactic mass of $(7.6 \pm 2.1) \times 10^{11}\ M_\odot$ interior to 6.7 R_0 found by Hartwick and Sargent (1978), assuming isotropic distribution of the globular cluster velocities, was converted to a rotation speed at that radius. Error bars on the rotation speed values for the tangent point data include the uncertainties in the fitted velocity centroid, spatial bin width, and velocity corrections. Those for the CO–H II data include the projection of the distance uncertainties along the galactocentric radial direction. All these data were binned in $\Delta R = 0.005\ R_0$ bins to match the CO survey data.

A composite curve was fitted by a polynomial of the form

$$\begin{aligned}
\theta(R) &= \sum_{i=0}^{6} A_i R^i , && R < 0.09\ R_0 , \\
&= \sum_{i=0}^{5} B_i R^i , && 0.09\ R_0 < R < 0.45\ R_0 , \\
&= \sum_{i=0}^{7} C_i R^i , && 0.45\ R_0 < R < 1.6\ R_0 , \\
&= D_0 , && 1.6\ R_0 < R , \quad (5)
\end{aligned}$$

with the additional constraints that the curve and its first two radial derivatives be continuous across the boundaries at 0.09, 0.45, and 1.6 R_0. The number of terms in each region was determined by the F-test and the locations of the boundaries found by minimizing the fit residuals. The coefficients of the polynomial for the two sets of constants corresponding to $(R_0, \theta_0) = (8.5$ kpc, 220 km s$^{-1})$ and (10 kpc, 250 km s^{-1}) and their uncertainties are listed in Table 3.

The combined observational data and uncertainties, these polynomials, and the BG rotation curve are shown in Figure 3 for both sets of the constants. The overall fits have computed uncertainties of 0.3–0.5 km s^{-1}, but inspection of the curves shows that these values are meaningful only interior to R_0. The fit in the outer portion is more uncertain and depends heavily on the choice of outer boundary radius and polynomial order. The curve in this region should be viewed as uncertain by 10–20 km s^{-1}. Southern hemisphere data would obtain curves different from the present ones by about 5 km s^{-1}. This value may be the best estimate of the true uncertainties.

The derived Oort constants for the two northern curves are:

$$\begin{aligned}
A &= \ \ 14.71 \pm 0.02 \text{ km s}^{-1} \text{ kpc}^{-1} , \\
B &= -10.27 \pm 0.02 \text{ km s}^{-1} \text{ kpc}^{-1} ,
\end{aligned} \quad (10 \text{ kpc}, 250 \text{ km s}^{-1}) ,$$

and

$$\begin{aligned}
A &= \ \ 17.68 \pm 0.03 \text{ km s}^{-1} \text{ kpc}^{-1} , \\
B &= -8.08 \pm 0.03 \text{ km s}^{-1} \text{ kpc}^{-1} ,
\end{aligned} \quad (8.5 \text{ kpc}, 220 \text{ km s}^{-1}) ,$$

where the uncertainties are from the formal fits and are lower limits, since the uncertainties in R_0 and θ_0 were not included and because the fits are largely controlled by the CO survey data (due to their smaller uncertainties) and only weakly by the data outside R_0. Realistic uncertainties are probably of the order of 0.5 km s^{-1} kpc^{-1}. The values of AR_0 derived here are 147.1 km s^{-1} (10 kpc) and 150.3 km s^{-1} (8.5 kpc), which are considerably steeper than the value of 126 km s^{-1} determined in § II*d* above.

IV. DISCUSSION

a) Large-Scale Features

There are regions in Figure 3 where the CO survey rotational velocities are very different from the best fit rotation curve. These are the large-scale features mentioned earlier. The fundamental difference between these motions and the cloud-cloud motions is illustrated in Figure 4. There, the velocity residuals of the inner Galaxy CO data, after subtracting the rotation curve, are plotted, along with the values of the cloud-cloud dispersion, versus Galactic radius. The formal value for the rms of the residuals is 4.8 km s^{-1}, but there are regions exhibiting motions to 10 and 15 km s^{-1}. The regions between 0.50–0.56 R_0, 0.73–0.80 R_0, and 0.97–1.0 R_0 possess large positive sys-

tematic motions with respect to the gas outside these radii. These have previously been identified with the Scutum, Sagittarius, and Local spiral arms respectively (Burton and Shane 1970; Shane 1972; Cohen *et al.* 1980). In CO longitude-velocity diagrams they stand out as bright CO at higher velocities than the neighboring material (see Robinson *et al.* 1984).

The periodic nature of the deviations in Figure 4*a* suggest that Fourier analysis might help quantify the characteristics of these motions. Figure 5 shows a power spectrum of the velocity residuals in Figure 4*a*. The wavelengths measured correspond to the galactocentric radial component of the distance between neighboring tangent points, and the velocities transformed are the residuals to the rotation curve, thus line-of-sight velocities. Since the true distance between points along the loci of tangents varies as sec l, the wavelengths in Figure 5 are lower limits. The only part of Figure 4*a* significantly affected by the sec l term is the local feature at 0.97–1.0 R_0, which is found to broaden to nearly the widths of the other two features. The dominant wavelengths in the power spectrum are at 0.22, 0.12, and 0.05 R_0. The first two lengths are due to the basic separation of the three regions noted, and the first harmonic of that separation. The magnitude of the 0.22 R_0 motion, projected along the line of sight, is about 5 km s^{-1}. The peak at 0.05 R_0 may be related to the width of the excess velocity regions, since it not a simple harmonic of the 0.22 R_0 wavelength. Whereas the three-dimensional value of the cloud-cloud dispersion is traditionally computed assuming independence of the motions along the three axes, the large-scale motions are correlated with position and likely also with direction. Thus, the large-scale motions seen here are characterized by minimum length scales of 0.22 R_0 and probably minimum velocities of 5 km s^{-1}.

b) *Cloud-Cloud Motions*

Previous measurements of the cloud-cloud velocity dispersion σ_{cc} have all suffered from contamination due to streaming motions. Stark (1984) arrived at the highest estimates of 7–9 km s^{-1}, by observing cloud motions toward the Galactic anticenter, a direction devoid of Galactic rotation effects, but not so clear of streaming. He has claimed that cloud-cloud motions and streaming are *both* characterized by small length scales and so cannot be easily separated observationally. The independence of the large-scale and small-scale motions shown in Figure 4 are at odds with Stark's interpretation. The smallest value previously obtained, 4.2 ± 0.5 km s^{-1}, by Liszt and Burton (1983), still relied on the assumption of *identical* (not merely similar) streaming behavior of the H I and CO components. Deviations from this assumption will cause their number to err above its true value. The lower value measured here, 3.0 km s^{-1}, and the relative smoothness of the cloud-cloud dispersions with galactocentric radius in Figure 4*b*, compared to the variations of the mean velocity residuals in Figure 4*a*, and the different relevant length scales found (0.015 versus

TABLE 3

COEFFICIENTS OF THE ROTATION CURVES[a]

Coefficient	$R_0 = 10$ kpc, $\theta_0 = 250$ km s^{-1}		$R_0 = 8.5$ kpc, $\theta_0 = 220$ km s^{-1}	
	$R/R_0 < 0.09$			
A_0[b]	0.0		0.0	
A_1	+2618.86	(41.)	+3069.81	(48.)
A_2	−11486.7	(430.)	−15809.8	(590.)
A_3	+27263.8	(1600.)	+43980.1	(2600.)
A_4	−36117.9	(2800.)	−68287.3	(5400.)
A_5	+24768.	(2300.)	+54904.	(5200.)
A_6	−6819.	(710.)	−17731.	(1900.)
	$R/R_0 = 0.09$–0.45			
B_0	+319.8354	(8.5)	+325.0912	(8.5)
B_1	−194.3591	(19.)	−248.1467	(22.)
B_2	+155.30181	(15.)	+231.87099	(21.)
B_3	−63.00332	(5.7)	−110.73531	(9.1)
B_4	+12.142556	(0.98)	+25.073006	(1.9)
B_5	−0.869573	(0.065)	−2.110625	(0.14)
	$R/R_0 = 0.45$–1.6			
C_0	−1931.3363	(120.)	−2342.6564	(120.)
C_1	+1768.47176	(103.)	+2507.60391	(120.)
C_2	−606.461977	(36.)	−1024.068760	(49.)
C_3	+112.102138	(6.6)	+224.562732	(11.)
C_4	−11.9698505	(0.71)	−28.4080026	(1.3)
C_5	+0.7367828	(0.044)	+2.0697271	(0.097)
C_6	−0.02423453	(0.0014)	−0.08050808	(0.0038)
C_7	+0.00032952	(0.000019)	+0.00129348	(0.000061)
	$R/R_0 > 1.60$			
D_0	264.76	(1.6)	234.88	(1.8)

[a] All errors are probable errors, 0.67 σ.
[b] This coefficient assumed.

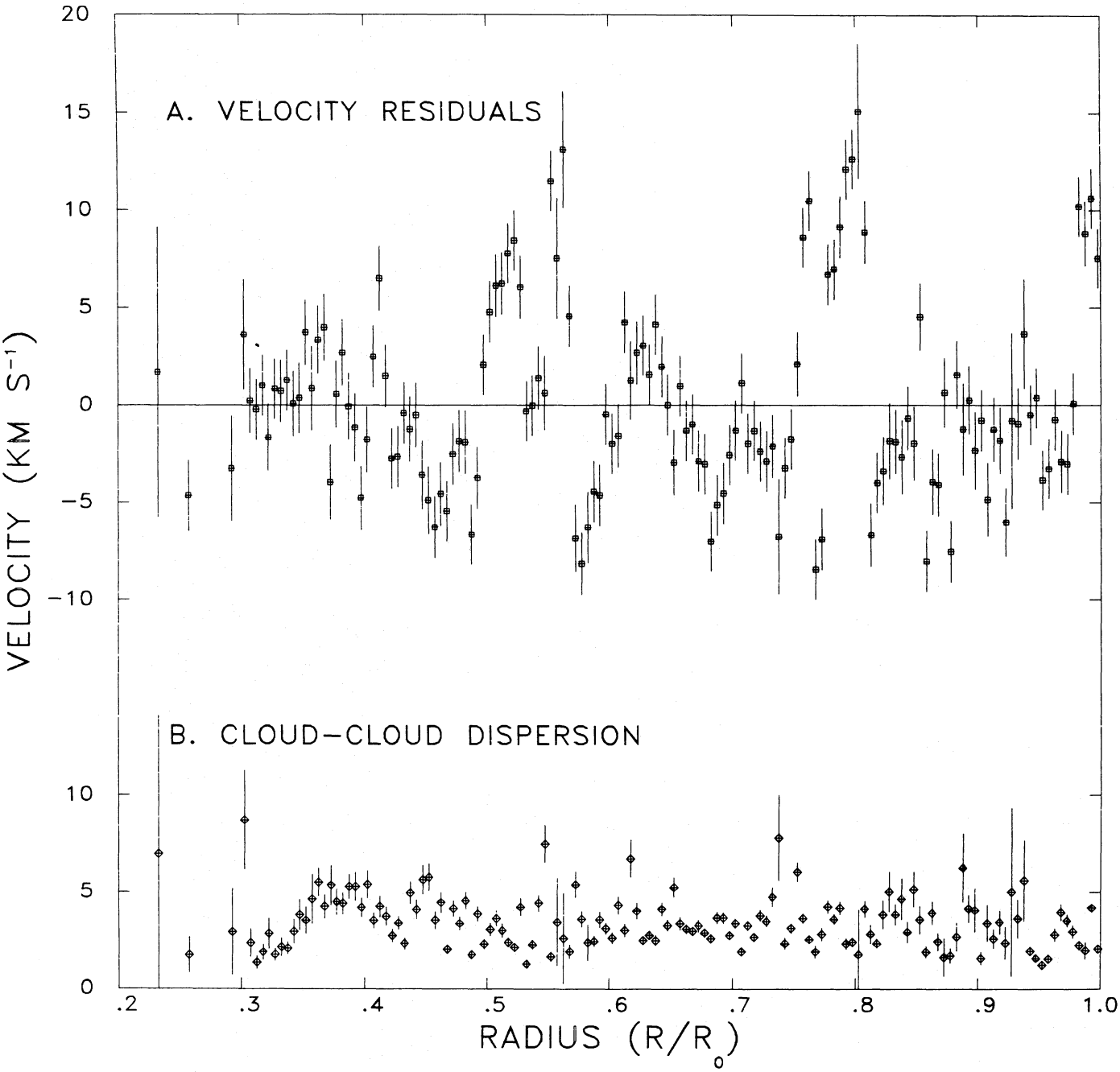

FIG. 4.—(*a*) Velocity residuals to the rotation curve, for the inner Galaxy CO data, vs. radius. (*b*) Cloud-cloud dispersion vs. radius.

0.22 R_0), indicate that these motions have been successfully separated.[3]

The cloud-cloud dispersions in Figure 4*b* might be expected to vary with position in the Galaxy. A variation is seen in the $\pm 2\sigma_z$ and unrestricted latitude samples. The dispersions in these samples possess significant gradients with Galactic radius: σ_{cc} varies from 4 km s^{-1} at 0.2 R_0 to 2.5 km s^{-1} at R_0. The more restricted samples do not show such a gradient, indicating that positional dependence of the dispersion may be the result of contamination, as discussed earlier, or a z-height effect, as might be expected of an ensemble of clouds exhibiting equipartition of energy. Blitz, Magnani, and Mundy (1984) find a cloud-cloud dispersion of 5.7 ± 1.2 km s^{-1} for their local sample of high-latitude molecular clouds. If molecular clouds do exhibit equipartition of energy, their smaller clouds (mean size ~2 pc) should have a larger value of σ_{cc} and a larger scale height. This is consistent with the increase in σ_{cc} found for the wider latitude samples here. Along the CO midplane there is no significant radial gradient in the cloud-cloud dispersions, indicating that streaming motions are probably not strongly coupled to cloud-cloud motions.

[3] The spikes at 0.55 and 0.73 R_0 in σ_{cc} in Fig. 4*b* are associated with the rapid onset and decay of the large-scale motions there. In these regions, the large-scale and cloud-cloud motions are blended in the bins used. Smaller binning removes these features from σ_{cc}.

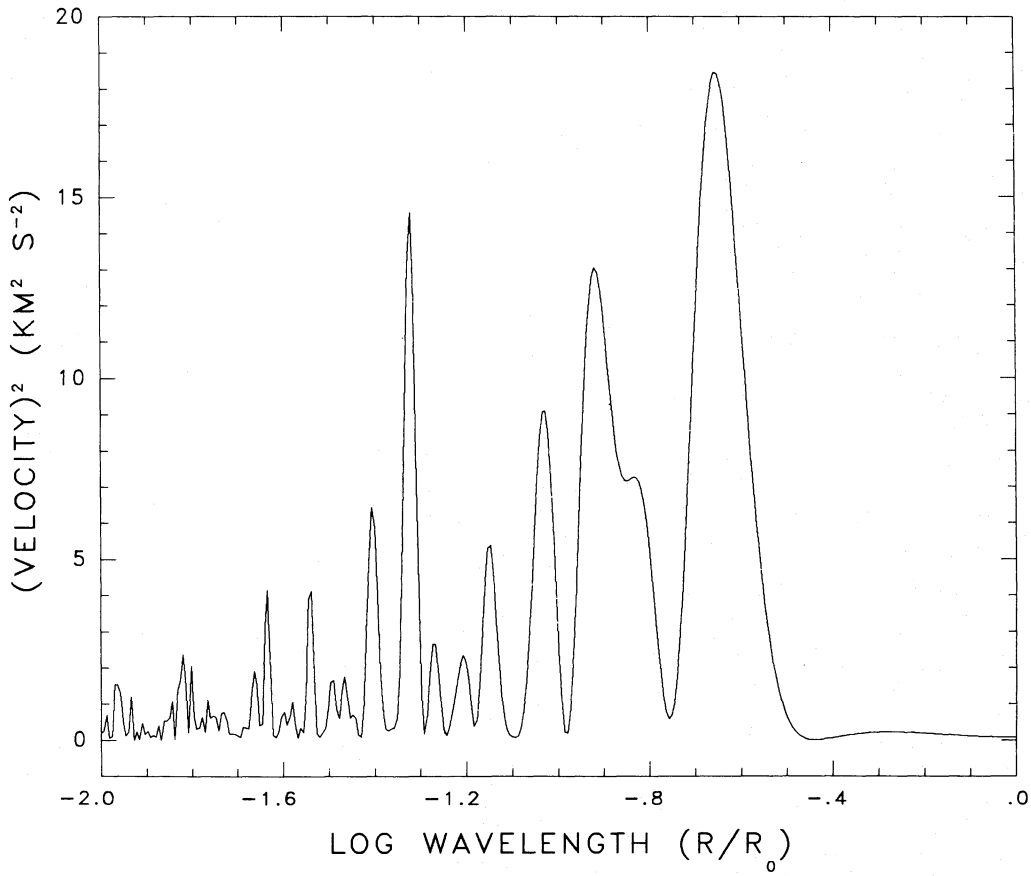

FIG. 5.—Power spectrum of the velocity residuals of Fig. 4*a*. Wavelength is measured along the galactocentric radial direction only. Note the features at 0.22, 0.12, and 0.05 R_0 (log wavelengths ≈ -0.65, -0.78, and -1.33).

c) LSR Motion

Recently, Stark (1984) has attempted to solve for the LSR motion based on the distribution of CO cloud peculiar velocities as a function of Galactic longitude. Belfort and Crovisier (1984) have used observations of nearby H I clouds to infer no significant peculiar motion of the LSR. Inspection of the last few data points in Figure 2 shows that *locally*, i.e., for Galactic radii between 0.975 and 1.0 R_0, large-scale motions are present. Samples of local clouds, such as the ones of Stark or of Belfort and Crovisier, will possess members outside this local perturbation region as well as within it. Stark and Blitz, Fich, and Stark (1980) obtain higher values of σ_{cc} than that found here. This may be a reflection of the mixing of the large and small-scale motions in their samples due to the local velocity perturbation.

There is no consensus regarding the *radial* motion of the LSR. Typical values range from 0 to 7 km s^{-1}. The failure of the test mentioned in § II*c* leads to no correction being applied to the current data. Future accurate determination of this motion requires identification of a sample of objects *outside* the local velocity perturbation. The CO–H II regions surveyed by Blitz, Fich, and Stark (1982) may be such objects, but completeness problems interior to R_0 will pose difficulties.

d) Tangent Point Schemes

The original reason for pursuing this study was to answer the question of whether determination of the rotation curve along $b = 0°$, as was done by BG, was an accurate determination. This was tested using the current data by comparing the tangent detections along $b = 0°$ to the Gaussian tangent components listed in Table 2. Figure 6 shows the velocity difference ($V_{b=0} - V_{\text{Gaussian}}$) histogram obtained from the sample of 787 $b = 0°$ detections at 1.2 K. For the 2 km s^{-1} binning used, the indicated Gaussian is centered at 0.3 ± 0.1 km s^{-1} and its dispersion is 4.3 ± 0.1 km s^{-1}. Since this method, in principle, is identical to the H I–^{13}CO difference spectrum formed by Liszt and Burton (1983) for longitudes between 20° and 40°, the similarity of the dispersions is not surprising. Determination of the tangent point along $b = 0°$ will therefore not err in the mean but will possess larger errors and noisier data than the method presented in § II.

The BG data, which do not include the peculiar LSR motion correction, when fitted, lead to a rotation curve which passed through the point at (R_0, θ_0). When the data of Table 2 are corrected for the 3 km s^{-1} line widths to 1.2 K and compared to the BG rotation curve, the mean difference is 4.275 ± 0.002 km s^{-1}. As the tangent velocity at $b = 0°$ has been shown to be within 0.3 km s^{-1} of the $\pm 1\sigma_z$ tangent velocity (in the mean), there remains a difference of some 4 km s^{-1}. This is probably due to the different tangent point detection schemes used: the "equivalent rectangular measure" of Shane and Bieger-Smith (1966) applied by BG versus the line edge scheme used in § II. A similar difference between these two methods was discussed by GKT for H I rotation curves, and the comparison between CO and H I is further complicated by the different dispersions of the H I and CO lines. Each H I velocity from BG used in

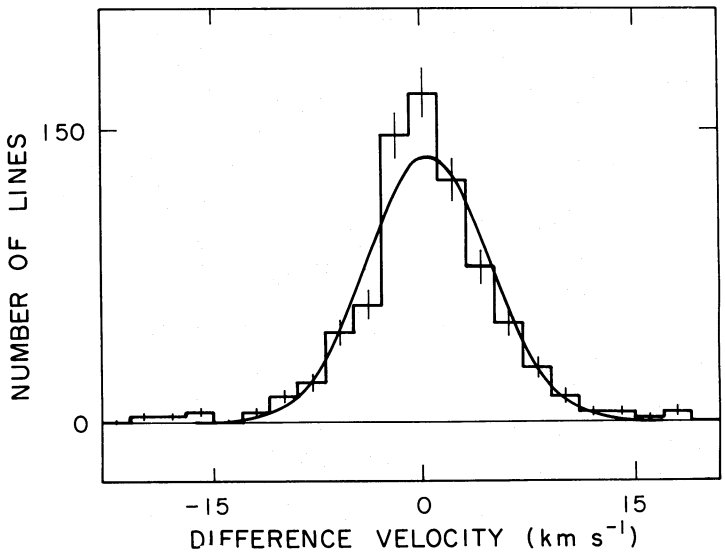

FIG. 6.—Distribution of the velocity differences between tangent point detections at $b = 0°$ only and the Gaussian tangent points of Table 2. The 787 $b = 0°$ detections have a mean only 0.3 ± 0.1 km s^{-1} higher than the $\pm 1\sigma_z$ sample, with a dispersion of 4.3 ± 0.1 km s^{-1}, in the 2 km s^{-1} channels used here.

calculating the combined rotation curve was therefore reduced by 4 km s^{-1} before correcting for the LSR motion (as noted in § II). The uncertainties in this value are tied to those of the line width correction for CO (~ 1.5 km s^{-1}), though firm lower and upper limits of 3 and 6 km s^{-1} for the correction may be similarly argued.

e) *Assumptions*

Several assumptions were needed to convert the measured velocities of the last 1.2 K channel in each CO survey spectrum to the final rotation curve. The first involved the extrapolation of the Sanders, Scoville, and Solomon (1985) line width and size distributions to below 20 pc. If the size distribution turns over shortward of 20 pc, the mean line width increases and the desired correction to the measured velocities is increased. Similarly, if the power index on the distribution is flatter than their -2.32 value (Clemens 1985), the correction is also increased. The correction calculated assuming a Gaussian line shape is certainly incorrect, as the CO lines seen toward molecular clouds are always optically thick. However, this effect operates in an opposite sense to the previous (probable) turnover in the size extrapolation, reducing the error contributed by each assumption. The velocity correction does affect the rotation curve directly, though firm lower and upper limits of 2 and 5 km s^{-1} keep the error introduced modest. The cloud-cloud dispersions are unaffected by this factor. By far the worst assumption here is in allowing a mean correction to be applied. Cloud properties vary a great deal from cloud to cloud, and the best approach would be to fully isolate each tangent cloud and then study the ensemble of these clouds. Unfortunately, line blending precludes such an approach.

In assigning meaning to the $N(v)$ distributions formed, the simplification that each cloud only contributed one velocity and one line was used. However, large clouds at the tangent point will tend to preferentially populate certain channels in the $N(v)$ spectra, notably the ones eventually associated with the Gaussian velocity center. For a collection of clouds exhibiting equipartition of energy, the biggest clouds will *define* the velocity centroid by possessing the lowest velocity difference with respect to the mean, and by contributing more lines to the $N(v)$ spectra than an average cloud. The net effect is a reduction of the dispersion of the fitted Gaussian with respect to the true gas motions, with no first-order effect on the velocity mean.[4] Countering this is the positional variation in the measured center velocities of clouds (see maps in Sanders *et al.* 1985). Successive measurements of a single cloud at several positions will contribute a non-vanishing dispersion to $N(v)$ characteristic of the *intrinsic* velocity jitter within the cloud. The large numbers of lines measured here allows good determination of the wings of the $N(v)$ distributions, which are crucial to determining the correct dispersion, especially in light of the contamination problems from clouds not at the tangent point. As mentioned, these contaminations generally occur on the low-velocity side of the tangent Gaussian, so resolving the high-velocity wing is the key to an accurate measurement of the cloud-cloud motions.

The large-scale motions of § IV have been identified as arising from motion ordered over length scales of $0.22\ R_0$, of which streaming, possibly associated with spiral arms, is the most obvious candidate. An alternate explanation for these velocities above the mean rotational velocity is that they represent *orbital* velocities about very massive molecular cloud complexes. Although the details are being investigated elsewhere (D. B. Sanders, private communication), the expected orbital velocities for clouds 40–50 pc from a $10^7\ M_\odot$ cloud complex are of the same order of magnitude as the perturbations found in § IV. The basic length scale, $0.22\ R_0$, might then represent the mean distance between such complexes. Significant in this regard is the comparatively smooth appearance of the CO residuals outside these perturbed regions.

The dip in the rotation curves near $0.3\ R_0$ and the peak at smaller radii may not accurately reflect the true circular motions of gas at these radii. The "3 kpc expanding arm" and other nuclear features may possess significant noncircular velocities which undermine the interpretation of tangent emission for radii less than about $0.3\ R_0$.

[4] Such an effect is probably present in the center channels in Fig. 6, which deviate from the Gaussian fit in the manner predicted.

f) *Outer Galaxy*

The dip in the rotation curves just outside R_0 may be an artifact of large-scale motions associated with the Perseus spiral arm. However, Sancisi (1983) has observed similar dips in galaxies, usually signifying changes in the disk gas properties including warping. Warps in the outer Galaxy H I layer have recently been studied by Kulkarni, Blitz, and Heiles (1982) and Henderson, Jackson, and Kerr (1982).

The detailed behavior of the rotation curve beyond 1.5 R_0 is open to question. The choice of constant rotation speed is guided by the observations of the rotation curves in other Sb and Sc galaxies (Rubin, Ford, and Thonnard 1978, 1980; Rubin *et al.* 1982), which show no curves which decrease with radius. From an analysis of globular cluster data, Frenk and White (1980) argue for a flat or rising rotation curve for the Galaxy, and against the Galactic mass derived by Hartwick and Sargent (1978) assuming radial globular cluster orbits. (This mass is smaller by a factor of 2.2 than the mass found assuming isotropically distributed velocities.) The rotation curve used by Caldwell and Ostriker (1981), which is constrained at 60 kpc by the logarithmic average of the two Hartwick and Sargent masses, seems too low in the outer Galaxy and has no counterparts in the Sb and Sc rotation curves. However, Pier (1984) has recently studied the kinematics of several types of halo objects and finds a radial-to-axial velocity anisotropy ratio of 2:1. Bahcall, Schmidt, and Soneira (1982) have produced model rotation curves flat to 1 km s^{-1} from 40 to 60 kpc, but with the halo density falling as $R^{-2.7}$ instead of the usual R^{-2}. Using an analysis of gravitational lensing by distant galaxies, Tyson *et al.* (1984) find that spiral galaxy masses and average rotation speeds are much less than those in the samples selected by Rubin, Ford, and Thonnard. These studies may argue for a somewhat lower Galactic mass than the value used here to limit the rotation curve at large radii.

V. SUMMARY

The new Massachusetts–Stony Brook Galactic plane CO survey and previously published H I, outer Galaxy CO–H II regions, and globular cluster data have been combined to determine a rotation curve for the northern disk component of the Galaxy.

In addition to Galactic rotation, the inner Galaxy CO data exhibit the effects of streaming motions, with minimum wavelengths of 0.22 R_0 and probably minimum velocities of 5 km s^{-1}, and cloud-cloud motions with characteristic velocity dispersions of 3.0 km s^{-1}, and correlation lengths of about 0.015 R_0.

The LSR is found to have a noncircular component of velocity in the direction $l = 90°$ of magnitude 7 ± 1.5 km s^{-1}.

This work has been substantially improved because of critical readings by Drs. D. B. Sanders, L. Blitz, J. Kwan, and W. B. Burton. In addition to carefully reading several versions of this paper, Dr. Nick Scoville has served as my thesis advisor and steered much of my research, for which I am deeply in his debt. The Massachusetts–Stony Brook CO Survey and this current work have been greatly aided by Dr. Conrad Wogrun's commitment to graduate student access to large computers.

Note added in proof.—Dr. F. Sloff of Leiden Observatory has kindly pointed out that round-off errors in the polynomial coefficients contained in the preprint lead to 50 km s^{-1} errors at 1.6 R_0. The coefficients listed here in Table 3 are not rounded and lead to agreement at 1.6 R_0 to better than 1 km s^{-1}.

REFERENCES

Bahcall, J. N., Schmidt, M., and Soneira, R. M. 1982, *Ap. J.* (*Letters*), **258**, L23.
Belfort, P., and Crovisier, J. 1984, *Astr. Ap.*, **136**, 368.
Blitz, L. 1979, *Ap. J.* (*Letters*), **231**, L115.
Blitz, L., Fich, M., and Stark, A. A. 1980, in *Interstellar Molecules*, ed. B. H. Andrew (Dordrecht: Reidel), p. 213.
———. 1982, *Ap. J.* (*Suppl.*), **49**, 183.
Blitz, L., Magnani, L., and Mundy, L. 1984, *Ap. J.* (*Letters*), **282**, L9.
Burton, W. B., and Gordon, M. A. 1978, *Astr. Ap.*, **63**, 7 (BG).
Burton, W. B., and Shane, W. W. 1970, in *IAU Symposium 38, The Spiral Structure of Our Galaxy*, ed. W. Becker and G. Contopoulos (Dordrecht: Reidel), p. 397.
Caldwell, J. A. R., and Ostriker, J. P. 1981, *Ap. J.*, **251**, 61.
Clemens, D. P. 1985, Ph.D. thesis, University of Massachusetts at Amherst.
Cohen, R. S., Cong, H., Dame, T. M., and Thaddeus, P. 1980, *Ap. J.* (*Letters*), **239**, L53.
Frenk, C. S., and White, S. D. M. 1980, *M.N.R.A.S.*, **193**, 295.
Gunn, J. E., Knapp, G. R., and Tremaine, S. D. 1979, *A.J.*, **84**, 1181 (GKT).
Hartwick, F. D. A., and Sargent, W. L. W. 1978, *Ap. J.*, **221**, 512.
Henderson, A. P., Jackson, P. D., and Kerr, F. J. 1982, *Ap. J.*, **263**, 116.
Jackson, P. D., FitzGerald, M. P., and Moffat, A. F. J. 1979, in *IAU Symposium 84, The Large-Scale Characteristics of the Galaxy*, ed. W. B. Burton (Dordrecht: Reidel), p. 221.
Kerr, F. J. 1962, *M.N.R.A.S.*, **123**, 327.
Kulkarni, S. R., Blitz, L., and Heiles, C. 1982, *Ap. J.* (*Letters*), **259**, L63.
Kwee, K. K., Muller, C. A., and Westerhout, G. 1954, *Bull. Astr. Inst. Netherlands*, **12**, 211.
Liszt, H. S., and Burton, W. B. 1983, in *Kinematics, Dynamics and Structure of the Milky Way*, ed. W. L. H. Shuter (Dordrecht: Reidel), p. 135.
Liszt, H. S., Xiang, D., and Burton, W. B. 1981, *Ap. J.*, **249**, 532.
Pier, J. R. 1984, *Ap. J.*, **281**, 260.
Robinson, B. J., Manchester, R. N., Whiteoak, J. B., Sanders, D. B., Scoville, N. Z., Clemens, D. P., McCutcheon, W. H., and Solomon, P. M. 1984, *Ap. J.* (*Letters*), **283**, L31.
Rubin, V. C., Ford, W. K., and Thonnard, N. 1978, *Ap. J.* (*Letters*), **225**, L107.
———. 1980, *Ap. J.*, **238**, 471.
Rubin, V. C., Ford, W. K., Thonnard, N., and Burnstein, D. 1982, *Ap. J.*, **261**, 439.
Sancisi, R. 1983, in *Internal Kinematics and Dynamics of Galaxies*, ed. E. Athanassoula (Dordrecht: Reidel), p. 55.
Sanders, D. B. 1981, Ph.D. thesis, State University of New York, Stony Brook.
Sanders, D. B., Clemens, D. P., Scoville, N. Z., and Solomon, P. M. 1985, *Ap. J. Suppl.*, submitted.
Sanders, D. B., Scoville, N. Z., and Solomon, P. M. 1985, *Ap. J.*, **289**, 373.
Sanders, D. B., Solomon, P. M., and Scoville, N. Z. 1984, *Ap. J.*, **276**, 182.
Schmidt, M. 1965, in *Stars and Stellar Systems*, Vol. **5**, *Galactic Structure*, ed. A. Blaauw and M. Schmidt (Chicago: University of Chicago Press), p. 513.
Shane, W. W. 1972, *Astr. Ap.*, **16**, 118.
Shane, W. W., and Bieger-Smith, G. P. 1966, *Bull. Astr. Inst. Netherlands*, **18**, 263.
Shuter, W. L. H. 1982, *M.N.R.A.S.*, **199**, 109.
Stark, A. A. 1984, *Ap. J.*, **281**, 624.
Tyson, J. A., Valdes, F., Jarvis, J. F., and Mills, A. P. 1984, *Ap. J.* (*Letters*), **281**, L59.
Westerhout, G. 1976, *Maryland-Bonn Galactic 21-cm Line Survey* (College Park, MD: University of Maryland).
Yuan, C. 1969, *Ap. J.*, **158**, 871.

DAN P. CLEMENS: Steward Observatory, Tucson, AZ 85721